Improving the Atmospheric Correction of OLCI over Turbid Waters by Using the SWIR band at 1016 nm and a new Baseline Residual Technique

Juan I. Gossn[1], Kevin G. Ruddick[2], Ana I. Dogliotti[1,3], and Ana L. Delgado[4,5]

[1]*Instituto de Astronomía y Física del Espacio (IAFE), Consejo Nacional de Investigaciones Científicas y Técnicas - Universidad de Buenos Aires (CONICET - UBA), Buenos Aires, Argentina.*
[2]*Remote Sensing and Ecosystem Modelling team, Operational Directorate Natural Environment, Royal Belgian Institute of Natural Sciences, Brussels, Belgium*
[3]*Instituto Franco-Argentino para el Estudio del Clima y sus No Impactos (UMI IFAECI/CNRS-CONICET-UBA), Buenos Aires, Argentina.*
[4]*Instituto Argentino de Oceanografía (IADO), Consejo Nacional de Investigaciones Científicas y Técnicas - Universidad Nacional del Sur (CONICET-UNS), Bahía Blanca, Argentina.*
[4]*Departamento de Geografía y Turismo, Universidad Nacional del Sur (UNS), Bahía Blanca, Argentina.*

Abstract

Since April 2016, the OLCI era has begun, providing a new opportunity for atmospheric correction of turbid waters due to its novel spectral band in the SWIR. This new band at 1016 nm, which is much less expensive for the mission than longer SWIR bands (such as MODIS' 1240, 1640 and 2130 nm bands) may give similar and even better performances than far-SWIR and NIR bands for turbid water atmospheric correction with suitable algorithm development. Although water absorption at this band is 6.9 and 11.8 times higher than at 865 and 779 nm NIR bands, it is still not enough to fully absorb the backscattered signal produced by suspended sediments in very turbid waters such as Río de la Plata (Argentina). This means that an alternative to the "black water" approach is needed for this sensor in this region which makes special use of the new SWIR band. In this work, we present an atmospheric correction for turbid waters developed for OLCI, based on Baseline Residuals (BLRs), i.e. spectral quantities computed from band triplets (in the same way as the Fluorescence Line Height algorithm) of Rayleigh-corrected reflectances in the Red/NIR/SWIR bands. The BLR algorithm is evaluated and compared to results obtained with standard atmospheric correction approaches, showing better general performance and spatial de-correlation between atmospheric and water signal. Although the algorithm has proven to yield satisfactory match ups of Total Suspended Matter (Delgado *et al.* [Ocean Optics XXIV, (2018)]), future efforts will be put in validating water reflectance using radiometric field measurements.

1 Introduction

The NASA standard atmospheric correction algorithm applied to MODIS (Moderate Resolution Imaging Spectroradiometer) imagery uses two bands in the NIR (Near Infra-Red) at 765

and 865 nm, assuming zero ("black water") or calculable water-leaving radiance contribution at these bands [11][27][1] [2]. This procedure might be effective over waters with low to moderate turbidity, but fails for extreme turbidity and alternative options are needed. Other schemes are used which apply the black water assumption using bands at the Short-Wave-Infra-Red (SWIR) (e.g. 1240, 1640 and 2130 nm in MODIS), where water absorption drastically increases recovering negligible water-leaving radiance even in highly turbid waters [29][26] . Although ESA's Ocean and Land Colour Instrument (OLCI) on Sentinel-3 lacks far-SWIR bands (e.g. 1240nm, 2130nm in MODIS), it incorporates a novel SWIR band at 1016 nm, which adds significant information on sediment content of water, but where black water assumption does not hold for extreme turbidities [16]. Due to this novel spectral disposition combined with bands from MERIS heritage, OLCI images are an opportunity to test alternatives to SWIR-based black water approaches for turbid water atmospheric correction.

In this work, we designed a pixel-by-pixel (PP) aerosol correction algorithm for turbid waters based on the OLCI Red-NIR-SWIR (RNS) bands, where we have identified "atmospheric invariant" spectral quantities which are sensitive to water reflectance but insensitive to aerosols, e.g. Philpot 1991 [22]. This approach is based on the fact that in the RNS range, aerosol reflectance is spectrally smoother than water reflectance [24]. At low and moderate turbidity, the spectral variability of RNS water reflectance follows closely the reciprocal of the pure water absorption coefficient [23]. For extremely turbid waters this spectral variability is reduced with flattening of the water reflectance spectrum as the asymptotic "saturation" reflectance is approached. This spectral flattening occurs first, for moderate turbidity, at the shorter red wavelengths [8] and then, for higher and higher turbidity, at higher and higher wavelengths with higher and higher pure water absorption. In this respect the bands from MERIS heritage at 620, 709, 779 and 865 nm are already useful for moderately turbid waters, but the new OLCI band at 1016 nm should theoretically be an advantage in extremely turbid waters because of the much higher pure water absorption at 1016nm. To calculate directly the water reflectance, assuming only that aerosol reflectance is spectrally smooth, a 'Baseline Residual" (BLR) algorithm is proposed here for Rayleigh-corrected reflectances at 3 RNS bands. A baseline is formed between the shortest and longest wavelength of the triplet and is subtracted from the middle wavelength to give the BLR. This approach is similar to that adopted, for example, in the Fluorescence Line Height product [21] and gives a quantity, the BLR, that is invariant under spectrally-linear (or sufficiently smooth) signal addition. By calculating three different atmospherically "quasi-invariant" BLRs, defined by the Rayleigh-corrected (RC) reflectances at triplets (620-709-779) nm, (709-779-865) nm and (779-865-1016) nm, it is then possible to calculate water reflectance in the RNS on a pixel-by-pixel basis even in the case of extremely turbid waters where the water reflectance is not linearly related to SPM concentration and where the water reflectance spectrum does not simply follow the reciprocal of the pure water absorption spectrum described in Ruddick *et al.* 2006[23].

2 Calibration/validation datasets

To calibrate and validate the algorithm, OLCI imagery from different turbid sites (Río de la Plata (RDP), Bahía Blanca (BBL, Argentina) and Belgian Coast (BLG), see Fig. 3) were used. OLCI L1B and L2 imagery were downloaded from the Copernicus Online Data Access (CODA) [4], and correspond to the processing baseline v2.23 [28]. The detailed list of scenes used to calibrate and test performance of the algorithm is shown in Tab. 1. Before entering the BLR calculations, two preliminary corrections were applied to the L1B images. The first

one was done to remove the salt and pepper artifacts called Prompt Particle Events (PPEs) from the TOA radiance values following the algorithm proposed by Gossn (in press.) [13], which are highly likely to occur over the South Atlantic Anomaly (i.e. where Río de la Plata is located)[13][5]. Secondly, the effect of Rayleigh scattering by air molecules is removed, called "Rayleigh Correction", using SeaDAS v7.5 [2][27], to give the Rayleigh-corrected (RC) reflectance at all OLCI bands of interest (product ρ_S in SeaDAS).

NASA and ESA standard atmospheric corrections were also applied to OLCI imagery to compare performances with the present scheme: i) *l2gen* script from NASA's SeaDAS ([2] [27]) was run with aerosol option "-2", i.e. assuming an iterative procedure to find the optimum aerosol model using bands 865 nm and 1016 nm (termed SeaDAS-2(865,1016) hereafter), and ii) ESA's standard atmospheric correction, that combines the Baseline Atmospheric Correction (BAC, [1]), which is essentially a NIR-based black-pixel approach, together with the Bright Pixel Atmospheric Correction (BPAC, [19]), which calculates first the NIR water reflectance from an iterative approach.

Apart from OLCI scenes, *in situ* above-surface radiometric measurements were used to compare between *in situ* and OLCI-derived BLRs. A total of 105 water reflectance measurements were selected from several field campaigns (2013-2016) performed in Río de la Plata (RDP) (Argentina), using the Analytic Spectral Devices (ASD FieldSpec FR) spectroradiometer, which works in the spectral range of 350:1:2500 nm and was used to measure upwelling and downwelling radiances, just above surface and downwelling irradiance (E_d^{0+}) inferred from measuring nadir radiance at a quasi-lambertian plaque and multiplying it by π. The measurement protocol is detailed in Knaeps *et al.* 2012 [16] and follows the generic "Abovewater method 2" of the NASA 2003 Ocean Optics Protocols [17].

3 Algorithm Theoretical Basis [1]

The aerosol correction scheme presented here is based on a series of spectral magnitudes denominated here Baseline Residuals (BLR), which are defined using triplets of spectral bands as the difference between the Rayleigh-corrected (RC) reflectances at the "middle" (M) band (i.e. of intermediate wavelength) and the value of the baseline formed by the signals at the left (L) and right (R) bands at this middle wavelength as follows

$$BLR[\lambda_L, \lambda_M, \lambda_R] = \rho_{RC}[\lambda_M] - BL[\lambda_M|\lambda_L, \lambda_R], \tag{1}$$

where L, M, R stands for the left, middle and right wavelengths of the triplet, $\rho_{RC}[\lambda_M]$ is the RC reflectance at λ_M and $BL[\lambda_M|\lambda_L, \lambda_R]$ is the baseline term, given by:

$$BL[\lambda_M|\lambda_L, \lambda_R] = \frac{\rho_{RC}[\lambda_L](\lambda_R - \lambda_M) + \rho_{RC}[\lambda_R](\lambda_M - \lambda_L)}{\lambda_R - \lambda_L} \tag{2}$$

Other precursor algorithms in the Ocean Color field that use BLRs, include the Fluorescence Line Height (FLH,[21]), the Floating Algal Index (FAI,[15]), the Maximum Chlorophyll Index for MERIS (MCI; [14]), or the Synthetic Chlorophyll Index of Shen *et al.* 2010[25]. All such approaches are similar in the sense that BLR indexes are essentially unaffected by undesirable signal such as aerosol and/or moderate sun glint (and hence to errors in the process of removal of this signal), since these components are generally spectrally smoother (thus have a low impact on BLRs) than the in-water signal, especially in the RNS range.

[1] A more detailed description of the theoretical basis can be found at Gossn *et al.* 2017 [12]).

In this study, we have chosen to use the RC reflectances computed from OLCI bands 620, 709, 779, 865 and 1016 nm, from which we obtained three successive BLRs: $BLR[620,709,779]$, $BLR[709,779,865]$ and $BLR[779,865,1016]$. These spectrally-close triplets of bands have been chosen in order to i) maximize the impact of the (turbid) water signal on BLRs, and simultaneously ii) minimize the impact of the atmospheric components. Other OLCI bands inside this spectral region were not considered, as they are strongly affected either by i) absorption of atmospheric components such as O_2 (oxygen) and H_2Ov (water vapour) or ii) by chlorophyll absorption and fluorescence.

In order to account for possible alteration of BLRs by the atmosphere an "equivalent transmittance" multiplicative factor correction was applied to the computed BLRs. These factors were previously computed in Gossn *et al.* 2017[12] and are based on a quasi-Single Scattering semi-analytic model [10] and coupled ocean-atmosphere radiative transfer simulations [20].

The *BLR* 3-tuple computed at each pixel is associated to the closest (in the Euclidean sense) *BLR* 3-tuple that corresponds to a calibration grid (see §4), and the corresponding water reflectance at 865 nm and 1016 nm is assigned to the given pixel. The aerosol reflectance at these two bands is then obtained from subtracting the corresponding calculated water signal.

Finally, a last correction is performed over the aerosol reflectance at 865 nm ($\rho_a(865)$) to restrain the derived aerosol reflectance ratio, $\varepsilon_a(865,1016) = \frac{\rho_a(865)}{\rho_a(1016)}$ inside the range of [0.85; 1.25]. These bounds were determined as the extreme values taken over a set of 82 different selected windows of size $15px \times 15px$ from OLCI-A scenes of clear water regions close to Río de la Plata, Bahía Blanca, North Sea, Yellow Sea, Amazonas and North Australia.

4 BLR vs. water reflectance relation

To study the relation between BLRs and turbid water reflectances, we decided to use a subset of OLCI imagery to achieve a plausible calibration dataset, in order to avoid systematic errors induced by calibrating the algorithm with data coming from other sources, such as *in situ* measurements or radiative transfer simulations. Also, the available *in situ* measurements are not enough to reconstruct the whole BLR space, spanned by OLCI imagery see Fig. 2. To build this dataset, a total of 13 sub-regions from 9 cloud-, sunglint- and haze-free scenes were selected from Río de la Plata (see Tab. 1). Over these subregions a non-operational atmospheric correction was applied to infer water reflectance at bands 865 nm and 1016 nm, based on estimating the atmospheric component from manually selected fixed clear water windows, close to the windows of interest, of 15×15 pixels, referred here on as "Fix-AC".

These "clear windows" were chosen to be as close as possible to the subregion of interest and totally free from water signal in the RNS (determined by visual inspection of the Rayleigh-corrected rasters). This simple aerosol removal assumes a spatially uniform atmospheric signal which is subtracted from the whole subregion of interest as follows:

$$\rho_w = \frac{\rho_{RC} - med(\rho_{RC}^{ClearWin})}{t[\lambda,\mu]}, \tag{3}$$

where ρ_w, ρ_{RC} and $med(\rho_a^{ClearWin})$ are the water reflectance, the RC reflectance and the median of the RC reflectance at the selected Clear Window, and a simple expression is used for the diffuse transmittance factor, $t[\lambda,\mu]$ (as applied by NASA OBPG in the absence of aerosol information, [18]), which depends on the air mass factor, μ and the Rayleigh optical thickness, $\tau_{Ray}[\lambda]$ [3]:

$$t[\lambda,\mu] = e^{-0.5\tau_{Ray}[\lambda]\mu} \tag{4}$$

Once this process is performed, the calibration dataset formed by the mentioned subregions is used to fit a calibration surface in BLR 3-dimensional sub-space, which is spanned by $BLR[620,709,779]$, $BLR[709,779,865]$ and $BLR[779,865,1016]$ (see Fig.2). The calibration surface is done by performing a 2-dimensional mesh-grid of "X" ($BLR[620,709,779]$) in the range $-0.0100:0.0005:0.0350$ and "Y" ($BLR[709,779,865]$) in the range $-0.0300:0.0005:0.0150$. The "Z" ($BLR[779,865,1016]$) values at each point of the grid are taken as the median of the Z values taken by the calibration dataset in the corresponding (X,Y) pair. To each calibration point a set of water reflectances values at 865nm and 1016nm is assigned taken as the median of the values that fall inside the corresponding voxel.

5 Atmospheric correction scheme: Summary

The following list (shown in Fig. 1) summarizes the atmospheric correction algorithm:

1. Rayleigh correction is applied using SeaDAS v7.5 software.
2. Baseline residuals ($BLR[620,709,779]$, $BLR[709,779,865]$ and $BLR[779,865,1016]$) are computed from the corresponding Rayleigh-corrected reflectances.
3. An equivalent transmittance factor correction is applied to account for slight atmospheric effects on BLRs [12].
4. For each pixel, the computed BLRs are matched to the nearest BLRs from a calibration grid. The corresponding water reflectances at 865 and 1016 nm are assigned to the pixel.
5. The aerosol/glint reflectance at these bands is obtained by subtracting the assigned water signal to the RC reflectance.
6. A final correction is performed over $\rho_a(865)$ to restrain $\varepsilon_a(865,1016)$ inside the reasonable range of [0.85; 1.25].
7. This approach may be extended to the whole range of bands of interest by subtracting the water signal retrieved and applying the clear pixel assumption to extrapolate the aerosol signal to shorter wavelengths [11] [27].

6 Results

Given the lack of math-ups between *in situ* radiometric measurements and OLCI data for the studied regions, the Fix-AC approach (see §4) was used as a "ground-truth" to validate the performance of the BLR-AC scheme (Fig. 3). Pixels inside the marked coloured boxes, corresponding to the most turbid parts of the validation images listed in Tab. 1 were selected. The three regions were selected as representative of extremely turbid (Fig. 3b) and moderately turbid (Fig. 3a,c) waters. Water reflectances derived from both approaches show very similar patterns and very small RMSD (Root Mean Square Difference) values in both cases. In the case of the $620nm$ band, ρ_w^{BLR-AC} values were obtained by using a simple linear aerosol extrapolation from the correction bands at 865nm and 1016nm.

Another profitable way of evaluating the performance of an atmospheric correction is through the analysis of the spatial correlation between the retrieved water and aerosol reflectances. Fig. 4 shows water and aerosol reflectances at 865 nm retrieved by BLR-AC from OLCI scene over Río de la Plata on 2016-06-08T13:09:51Z, together with standard atmospheric corrections: ESA's BAC/BPAC and NASA's SeaDAS-2(865,1016) (see §2). The most challenging region for atmospheric correction over RDP is the turbidity front adjacent to Buenos Aires Province Coast (Argentina) at around 35^o5 S 57^o0 W (marked as $0.8^o \times 0.8^o$ boxes, see Fig. 4, and Fig. 5 to see a zoom at the turbidity front region), where suspended sediment concentrations, turbidity and water reflectances at the RNS are maximum [9][7]. It is clearly seen how standard atmospheric corrections yield undesirable higher correlation between the water and aerosol signals (Fig. 4 b-c, also lower visible spatial correlation between water and aerosol rasters in the BLR-AC case, compared to BAC/BPAC and SeaDAS-2(865,1016)). In general terms, BAC/BPAC and SeaDAS-2(865,1016) underestimate water signal or simply do not converge to a numeric solution (i.e. NaNs, seen as magenta in Figs. 4-5 e, f, h, i).

7 Discussion and Conclusion

A novel atmospheric correction algorithm for highly turbid waters is presented for S3/OLCI, which is based on assuming that the spectral shape of water reflectances in the RNS OLCI bands centered at 620, 709, 779, 865 and 1016 nm remains mostly unchanged by atmospheric effects. This spectral shape is quantified through Baseline Residuals (BLRs, Eq.1) of the three consecutive triplets of the aforementioned bands. The algorithm that relates BLRs to water reflectances at 865 and 1016 nm was calibrated by using OLCI data from selected subregions of images from Río de la Plata (Argentina), which were atmospherically-corrected by a simple Fix Window Atmospheric Correction (Fix-AC) that assumes spatial homogeneity of the atmosphere (given very clear sky conditions and small horizontal distances) and computes the atmospheric reflectance from fixed windows of $15px \times 15px$ corresponding to clear water regions. The BLR atmospheric correction approach has the advantage that it is designed on the bases of very simple physical principles and is keen to conserve correct spectral shapes of water reflectances, due to the fact that it is precisely designed to respect the "BLRs" (i.e. convexities) of water reflectances. Although no *in situ* radiometric measurements from Río de la Plata are available during the OLCI era, Delgado *et al.* 2018 [6] performed a match-up analysis to compare TSM products using different atmospheric correction algorithms over the southern Buenos Aires Province inner and mid-shelf, yielding best results for the BLR-AC approach. Even though BLR approach was designed to be performed over OLCI imagery, it might be easily expandable to other sensors that have spectrally-close triplets of bands in the Red/NIR/SWIR, such as the planned Argentinean-Brazilian joint ocean colour satellite mission SABIA/MAR.

8 Acknowledgement

This research was funded by BELSPO (Belgian Federal Science Policy Office) HYPERMAQ (SR/00/335) and ANPCyT (Promotion of Science and Technology Agency, Argentina) ANPCyT PICT 2014-0455. The assistance of the first author to the XXIV Ocean Optics Conference was possible thanks to financial support provided by The Oceanography Society in consultation with the Ocean Optics XXIV Planning Committee. ESA and Copernicus are acknowledged for Sentinel-3A/OLCI imagery.

References

[1] Antoine, D. & Morel, A., (1999), A multiple scattering algorithm for atmospheric correction of remotely-sensed ocean colour (MERIS instrument): principle and implementation for atmospheres carrying various aerosols including absorbing ones, *International Journal of Remote Sensing*, 20, 1875-1916.

[2] Bailey, S.W., Franz, B.A., & Werdell, P.J. (2010). Estimation of near-infrared water- leaving reflectance for satellite ocean color data processing. Optics Express, 18, 7521–7527.

[3] Bodhaine, B. A.,Wood, N. B., Dutton, E. G., Slusser, J. R. (1999) On Rayleigh Optical Depth Calculations. *Journal of Atmospheric and Oceanic Technology*, vol. 16.

[4] Copernicus Online Data Access, EUMETSAT: *www.coda.eumetsat.int*

[5] D'Amico, G. Corsini, M. Diani, J. Nieke (2015), Prompt-particle-events in ESA's Envisat/MERIS and Sentinel-3/OLCI data: observations, analysis and recommendations. Master Thesis presented at the University of Pisa, Italy.

[6] Delgado, A.L., P. D. Pratolongo, J.I. Gossn, A.I. Dogliotti, M. Arena, D. Villagran, M. Fernández Severini (2018), Evaluation of derived total suspended matter products from Ocean and Land Colour Instrument Imagery (OLCI) in the inner and mid-shelf of Buenos Aires Province (Argentina), Extended Abstract submitted to the XXIV Ocean Optics Conference, Dubrovnik, Croatia, Oct. 7-12, 2018.

[7] Dogliotti, A.I., Ruddick, K., Nechad, B., and Lasta, C. (2011) Improving Water Reflectance Retrieval from MODIS Imagery in the Highly Turbid Waters of La Plata River. Proceedings of VI International Conference: Current problems in optics of natural waters (ONW 2011). Publishing House Nauka of RAS, 2011. p. 152. Russia. 6-10 September, 2011.

[8] Doxaran, D., J.-M. Froidefond, S. Lavender, P. Castaing (2002) Spectral signature of highly turbid waters Application with SPOT data to quantify suspended particulate matter concentrations, Remote Sensing of Environment 81 (2002) 149 – 161

[9] Framiñan, M., O. Brown (1996), Study of the Río de la Plata turbidity front, Part 1: Spatial and temporal distribution, *Cont. Shelf Res.*, 16, 1259– 1282, doi:10.1016/0278-4343(95)00071-2.

[10] Gordon, H. R. , O. B. Brown, R. H. Evans, J. W. Brown, R. C. Smith, K. S. Baker, and D. K. Clark, "A semianalytic radiance model of ocean color," J. Geophys. Res. 93(D9), 10909–10924 (1988).

[11] Gordon, H. R., Wang, M. (1994) Retrieval of Water-Leaving Radiance and Aerosol Optical Thickness over the Oceans with SeaWiFS: A Preliminary Algorithm., Applied Optics, 33, 443-452.

[12] Gossn, J.I., Ruddick, K.G., Dogliotti, A. I. (2017). Atmospheric correction of OLCI imagery over very turbid waters based on the RED/NIR/SWIR bands. 10.23919/RPIC.2017.8214356.

[13] Gossn, J.I. (in press.) Effect of Prompt Particle Events on OLCI Ocean Colour Imagery in the South Atlantic Anomaly: Detection and Removal, IEEE Geoscience and Remote Sensing Letters.

[14] Gower, J. and King, S. (2008). Satellite images show the movement of floating Sargassum in the Gulf of Mexico and Atlantic Ocean. Nature Proceedings hdl:10101/npre.2008.1894.1

[15] Hu, C. (2007) A novel ocean color index to detect floating algae in the global oceans. *Remote Sensing of Environment*, 113 2118–2129.

[16] Knaeps, E and Dogliotti, A.I, Raymaekers, D, Ruddick, K and Sterckx, S. (2012) In situ evidence of non-zero reflectance in the OLCI 1020 nm band for a turbid estuary. Remote Sensing of Environment, 10.1016

[17] Mueller, J. L., R. R. Bidigare, C. Trees, W. M. Balch, J. Dore, D.T. Drapeau, D. Karl, L. Van Heukelem, and J. Perl (2003) Ocean Optics Protocols For Satellite Ocean Color Sensor Validation, Revision 5, Volume V: Biogeochemical and Bio-Optical Measurements and Data Analysis Protocols, NASA/TM-2003-, National Aeronautical and Space administration Goddard Space Flight Space Center, Greenbelt, Maryland.

[18] Mobley, Curtis D., Jeremy Werdell, Bryan Franz, Ziauddin Ahmad, and Sean Bailey (2016) Atmospheric Correction for Satellite Ocean Color Radiometry, A Tutorial and Documentation of the Algorithms Used by the NASA Ocean Biology Processing Group.

[19] Moore, G.F., Aiken, J., and S.J. Lavender (1999). The atmospheric correction of water colour and the quantitative retrieval of suspended particulate matter in Case II waters: application to MERIS. International Journal of Remote Sensing 20(9): 1713-1733.

[20] Lenoble, J., M. Herman, J.L. Deuzé, B. Lafrance, R. Santer, D. Tanré (2007) A Successive Order of Scattering Code for Solving the Vector Equation of Transfer in the Earth's Atmosphere with Aerosols. Journal of Quantitative Spectroscopy & Radiative Transfer, 107 479-507.

[21] Letelier, R. M., Abott, M. R. (1996) An analysis of chlorophyll fluorescence algorithms for the Moderate Resolution Imaging Spectrometer (MODIS). Remote Sensing of Environment, 58, 215 - 223.

[22] W. Philpot (1991) The derivative ratio algorithm: Avoiding atmospheric effects in remote sensing, IEEE Transactions on Geoscience and Remote Sensing. DOI: 10.1109/36.79425.

[23] Ruddick K.G., V. De Cauwer, Y.-J. Park, G. Moore (2006) Seaborne measurements of near infrared water-leaving reflectance: The similarity spectrum for turbid waters Limnol. Oceanogr., vol. 51-2, pp. 1167-1179, doi:10.4319/lo.2006.51.2.1167

[24] Ruddick, K.G., Vanhellemont, Q. (2015) Use of the new OLCI and SLSTR bands for atmospheric correction over turbid coastal and inland waters. Submitted for the proceedings of the Sentinel-3 for Science Workshop held in Venice-Lido, Italy, 2-5 June 2015, ESA Special Publication SP-734.

[25] Shen, F., Y.-X. Zhou, D.-J. Li, W.-J. Zhu & M. S. Salama (2010) Medium resolution imaging spectrometer (MERIS) estimation of chlorophyll-a concentration in the turbid sediment-laden waters of the Changjiang (Yangtze) Estuary, International Journal of Remote Sensing, 31:17-18, 4635-4650, DOI: 10.1080/01431161.2010.485216

[26] Shi, W., Wang, M. (2007). Detection of Turbid Waters and Absorbing Aerosols for the MODIS Ocean Color Data Processing. Remote Sensing of Environment, vol. 110, pp. 149–161.

[27] Stumpf, R. P., R. A. Arnone, J. R. W. Gould, P. M. Martinolich, and V. Ransibrahmanakul (2003) A Partially Coupled Ocean-Atmosphere Model for Retrieval of Water-Leaving Radiance from SeaWiFS in Coastal Waters. NASA Tech. Memo. 206892 (pp. 51–59).

[28] S3 Mission Performance Centre (2017), Sentinel-3 Product Notice S3A.PN-OLCI-L2L.02, Issue/Rev Date 06/11/2017, https://sentinel.esa.int/documents/247904/2702575/Sentinel-3-OLCI-Product-Notice-Level-2-Land.

[29] Wang, M., Shi, W. (2007) The NIR-SWIR Combined Atmospheric Correction Approach for MODIS Ocean Color Data Processing. Opt. Express 15, 15722-15733.

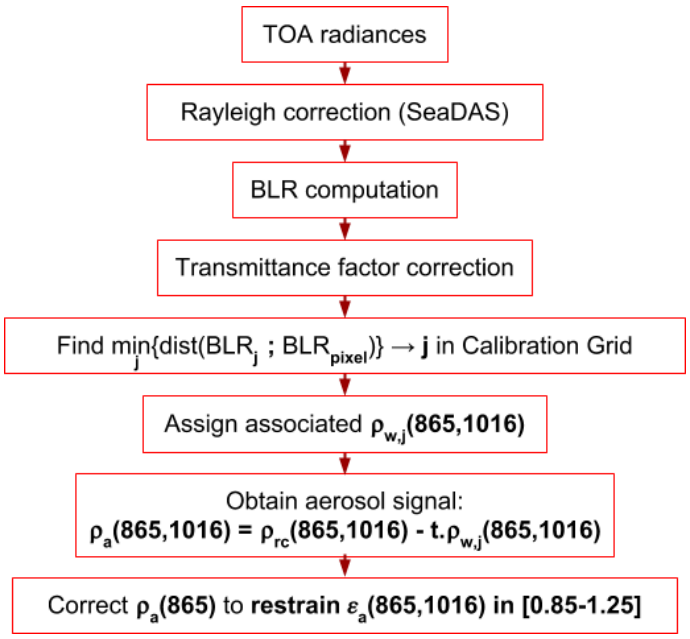

Figure 1: Scheme summarizing the BLR Atmospheric Correction (BLR-AC) approach, as listed in §5.

Table 1: List of OLCI scenes (L1B, processing Baseline v2.23) from Río de la Plata (RdP), Bahía Blanca, Argentina (BBl) and Belgian Coast (Blg) used to calibrate and validate the algorithm, together with the specific windows selected to build the calibration grid and perform the validation, and the clear water windows selected to perform the "Fix-AC" atmospheric correction (see §4).

Region	**Aquisition Date-Time** yyyy-mm-ddThh:mm:ssZ	**Cal/Val Window(s)** lines; pixels	**Fix-AC Window** lines; pixels	**Cal/Val**
RdP	2016-08-17T12:55:02Z	1347-1636; 1258-1528	1750-1764; 1143-1157	Cal
RdP	2016-11-10T12:51:59Z	1057-1446; 521-685	1598-1612; 567-581	Cal
RdP	2016-11-29T12:58:49Z	1643-1796; 1218-1332	2117-2131; 1267-1281	Cal
RdP	2017-01-14T13:06:26Z	2254-2589; 838-1052	2655-2669; 1155-1169	Cal
RdP	2017-03-13T13:02:29Z	1890-2013; 1177-1258 2044-2124; 1130-1256	2140-2154; 1462-1476	Cal
RdP	2017-05-01T13:32:08Z	4301-4525; 1126-1177 4381-4561; 1216-1356	4549-4563; 1271-1285	Cal
RdP	2017-07-02T13:24:47Z	3761-3840; 1220-1254	4133-4147; 1498-1512	Cal
RdP	2017-10-15T13:02:34Z	1586-1927; 1088-1182	2460-2474; 1635-1649	Cal
RdP	2017-11-19T12:54:31Z	1355-1576; 2252-2366 1367-1718; 2108-2247 862-1262; 2025-2108	1895-1909; 2178-2192	Cal
RdP	2017-10-31T12:47:47Z	724-927; 1398-1452	1104-1118; 1774-1788	Val (Fig. 3)
BBl	2016-10-09T13:22:33Z	2359-2701; 970-1094	2917-2931; 1077-1091	Val (Fig. 3)
Blg	2016-07-19T10:00:32Z	1613-1823; 1525-1649	1497-1511; 1790-1804	Val (Fig. 3)
RdP	2016-06-08T13:09:51Z	-	-	Val (Figs. 4-5)

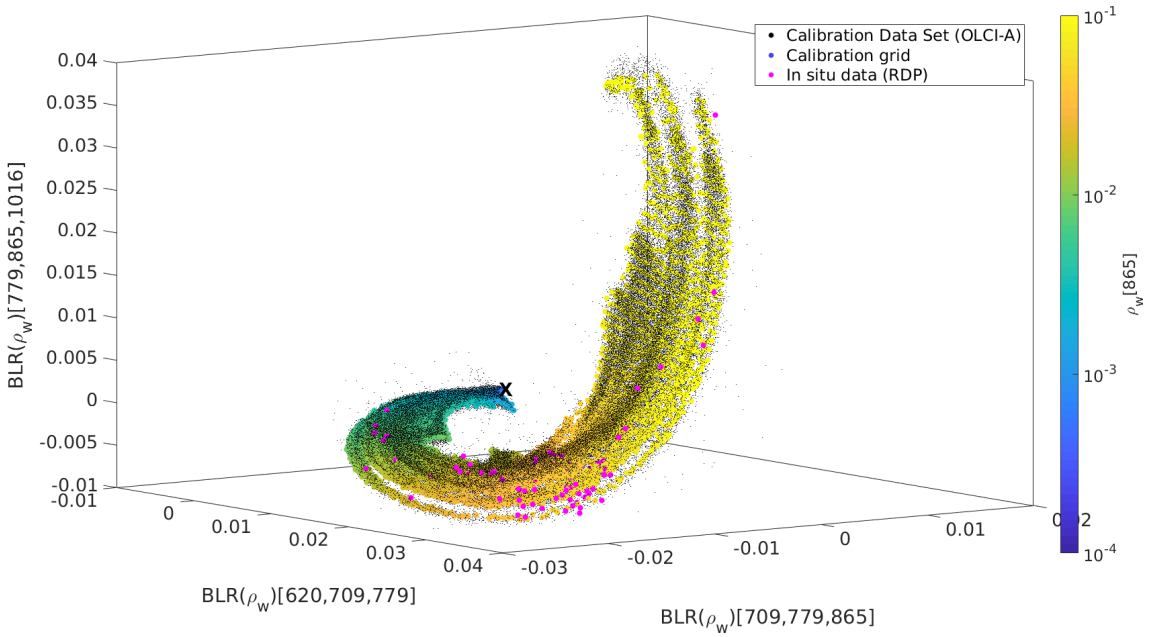

Figure 2: BLR space, formed by the three BLRs defined by the three consecutive triplets of the five OLCI bands 620 nm, 709 nm, 779 nm, 865 nm, 1016 nm. Small black dots: OLCI Calibration dataset (Tab. 1). Big color-mapped dots: Calibration grid obtained from the OLCI calibration dataset, whose color indicates water reflectance at 865 nm (see §4). Magenta dots are *in situ* radiometric data from Río de la Plata, which clearly fall inside the region spanned by the OLCI BLRs. An "X" indicates the origin, where BLR = 0, which corresponds to clear water scenarios.

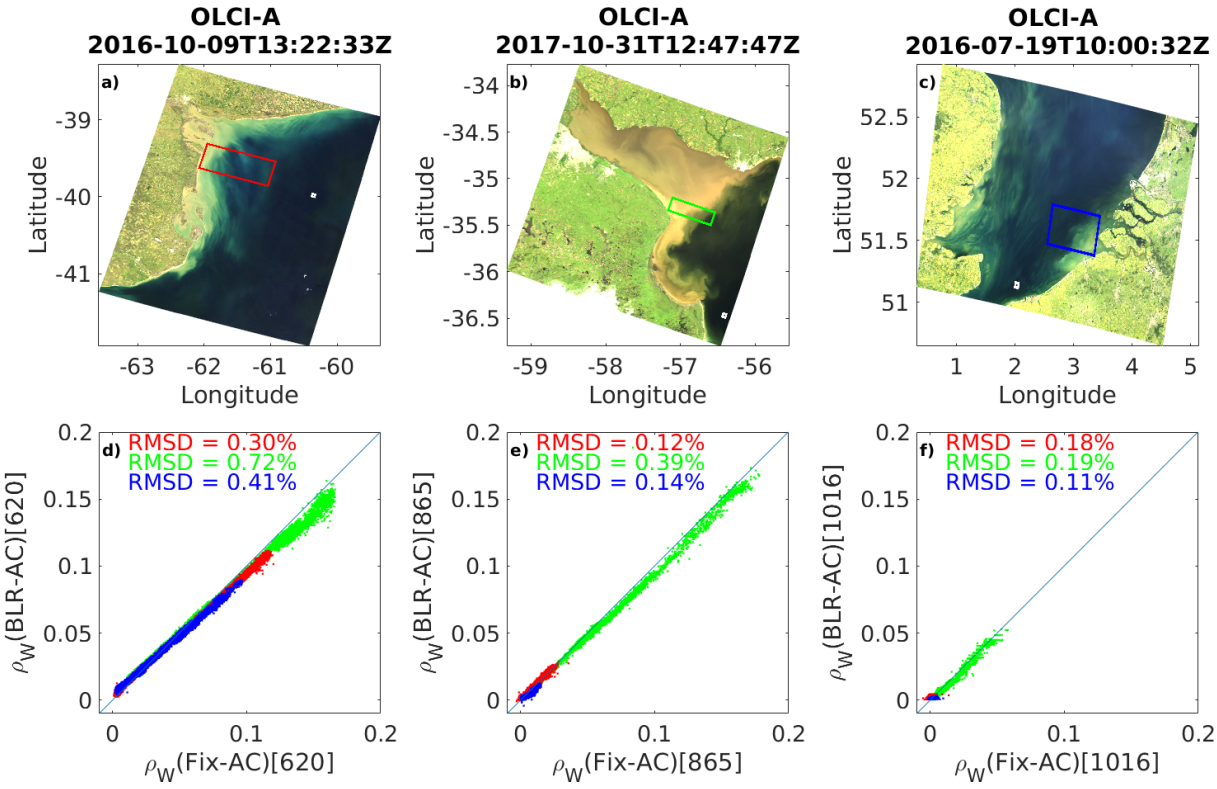

Figure 3: Intercomparison between BLR-AC and Fix-AC schemes. RGBs of scenes at Bahía Blanca (ARG), Río de la Plata and Belgian Coast from which the datasets are acquired (red, green and blue boxes at insets a-c, resp.). ρ_w^{BLR-AC} is plotted against ρ_w^{Fix-AC} for the selected boxes at bands 620 (d), 865 (e) and 1016 (f) nm. $\rho_w^{BLR-AC}[620]$ was estimated by assuming a simple linear aerosol signal extrapolation.

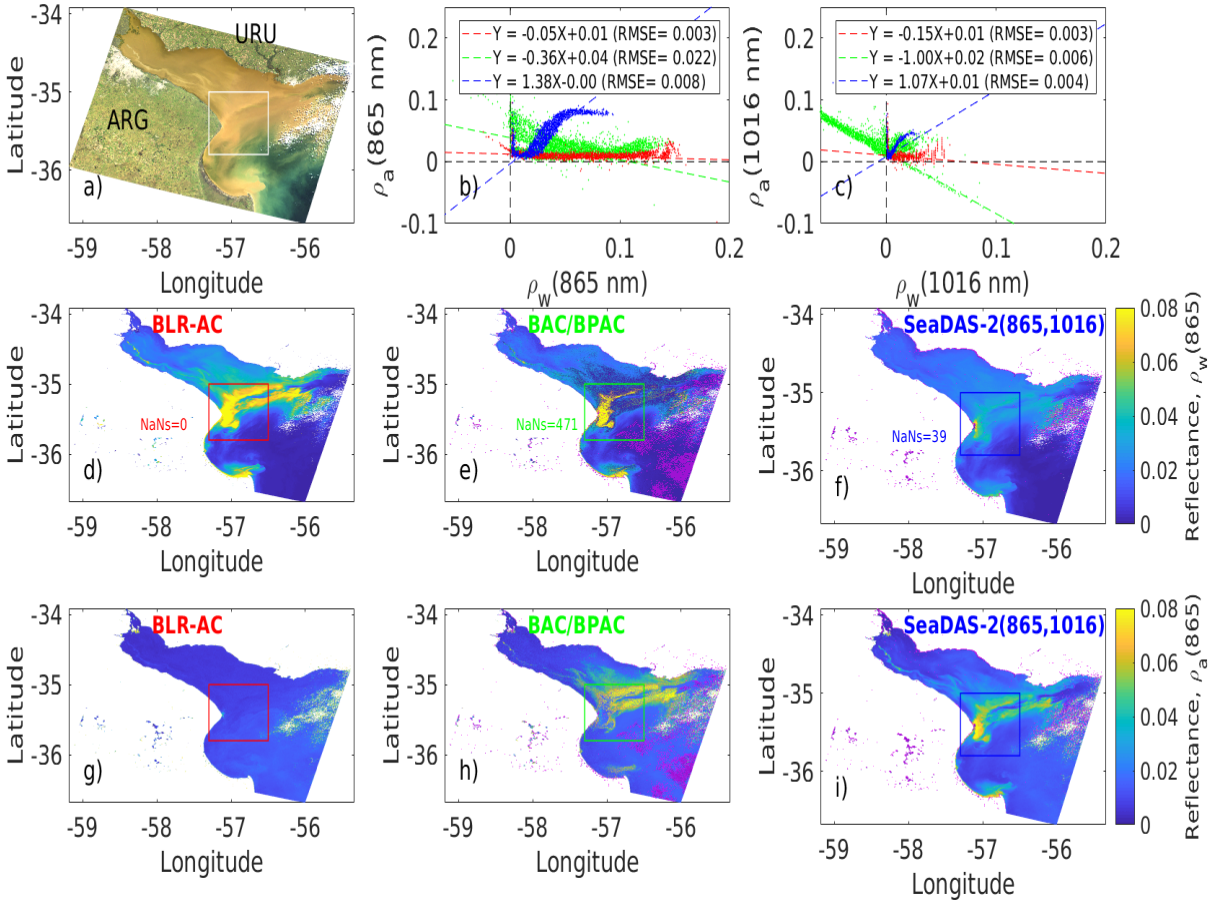

Figure 4: Comparison between atmospheric correction schemes BLR-AC, BAC/BPAC and SeaDAS-2(865,1016) performed over OLCI-A image acquired on 2016-06-08T13:09:51Z over Río de la Plata. a): RGB Composite. b)-c): Water vs. aerosol reflectances at 865/1016 nm over the turbid front subregion (marked with boxes of different colours corresponding to each scheme). d)-l): Water and aerosol reflectance at 865 nm, retrieved by: BLR scheme (d,g,h), OLCI's Baseline Atmospheric Correction (BAC/BPAC) (e,h,k) and SeaDAS iterative procedure using bands 865 and 1016 nm (SeaDAS-2(865,1016)) (f,i,l). NaN pixels are coloured in magenta.

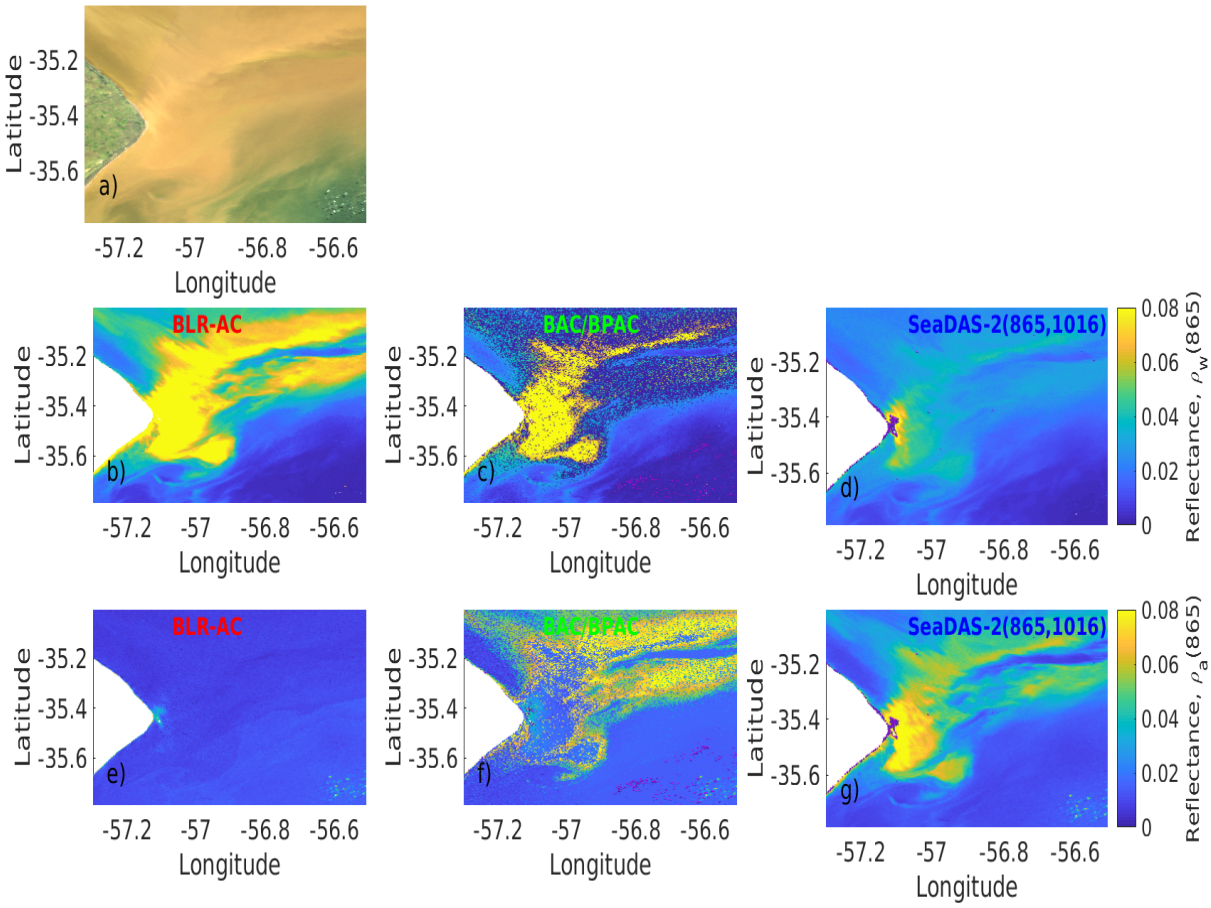

Figure 5: Same as 4, but zoomed over the Turbidity Front region.